Colloids and Surfaces A: Physicochem. Eng. Aspects 436 (2013) 380–385

Contents lists available at SciVerse ScienceDirect

Colloids and Surfaces A: Physicochemical and Engineering Aspects

journal homepage: www.elsevier.com/locate/colsurfa

Versatile one-pot synthesis of confeito-like Au nanoparticles and their surface-enhanced Raman scattering effect

Masaki Ujihara*, Toyoko Imae

Graduate Institute of Applied Science and Technology, National Taiwan University of Science and Technology, 43 Keelung Road, Taipei 10607, Taiwan

HIGHLIGHTS

- Confeito-like Au nanoparticles were obtained using H_2O_2 with various protectants.
- The nanoparticles had diameters ranging from tens to hundreds of nanometers.
- Morphologies of the particles differed by the protecting agents used.
- The nanoparticles displayed red-shifted and broadened plasmon absorption bands.
- Enhancing effect on Raman scattering depended on the morphology of nanoparticles.

GRAPHICAL ABSTRACT

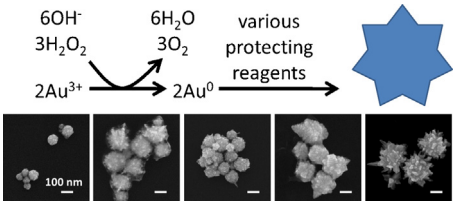

ARTICLE INFO

Article history:
Received 17 April 2013
Received in revised form 27 June 2013
Accepted 3 July 2013
Available online 11 July 2013

Keywords:
Gold nanoparticle
Confeito-like particle
Anisotropic nanoparticle
Localized surface plasmon
Surface-enhanced spectroscopy

ABSTRACT

A simple and versatile synthesis method for confeito-like Au nanoparticles was developed. Tetrachloroaurate was reduced by hydrogen peroxide in aqueous alkaline solutions in the presence of protecting agents. The reaction was accomplished within several hours at ambient temperature, and the Au nanoparticles obtained had confeito-like structures; however, their morphologies were slightly different from each other depending on the protecting agents (*polyvinylpyrrolidone*, *pluronic* surfactant, sodium dodecyl sulfate, citric acid, and hexadecyltrimethylammonium bromide) used. These nanoparticles had diameters ranging from tens to hundreds of nanometers, and they displayed red-shifted and broadened plasmon absorption bands as compered to spherical Au nanoparticles. The Au nanoparticles were accumulated on anodized alumina filters, and the surface-enhanced Raman scattering spectra of Rhodamine 6G were measured using excitation light with a wavelength of 785 nm. The enhancing effect was stronger for confeito-like structures than for polyhedral Au nanoparticles, and its order is almost the same as that of the plasmon absorption band.

1. Introduction

Metallic nanoparticles have been used as pigments for a long time, but their unique optical behaviors have been receiving a lot of attention recently [1,2]. Metallic nanoparticles have free electrons on their surfaces that can be oscillated by external electric fields. The wave of free electrons, the so-called "surface plasmon," resonates with the incident light. This "surface plasmon" is concentrated at junction points of the nanoparticles and projecting points of the surface, which are called "hot spots" [1–3]. Adsorbates on the hot spots can be efficiently excited, and this excitation results in

Abbreviations: AuNP, Au nanoparticle; Cit, citric acid; HTAB, hexadecyltrimethylammonium bromide; PF127, Pluronic F-127 a polyethylene oxide–polypropylene oxide–polyethylene oxide block copolymer; PVP, polyvinylpyrrolidone; R6G, rhodamine 6G; SDS, sodium dodecyl sulphate; SEIRAS, surface-enhanced infrared absorption spectroscopy; SEM, scanning electron microscopy; SERS, surface-enhanced Raman scattering spectroscopy; TEM, transmission electron microscopy; UV–vis–NIR, ultraviolet–visible–near infrared.

* Corresponding author. Tel.: +886 22730 3773; fax: +886 22730 3733.
E-mail addresses: masaki.ujihara@mail.ntust.edu.tw, masaki.ujihara@gmail.com (M. Ujihara).

0927-7757/$ – see front matter © 2013 Elsevier B.V. All rights reserved.
http://dx.doi.org/10.1016/j.colsurfa.2013.07.003

greatly enhanced spectra [3,4]. Such techniques are used for ultrasensitive analysis and are collectively known as surface-enhanced spectroscopy, surface-enhanced Raman scattering spectroscopy (SERS) [5], and surface-enhanced infrared absorption spectroscopy (SEIRAS) [6,7]. Although the rough surfaces and aggregates of nanoparticles of noble metals can enable the detection of Raman scattering from a single molecule [8], the enhancement factor is not reproducible because of their undefined structures. Therefore, methods to control the shapes [9–15] and aggregations [16,17] of nanoparticles have been examined to achieve a reliable and strong surface-enhanced effect. In the last several years, anisotropic nanoparticles have been developed and found to have strong SERS effects [18]. Although various nanostructures have been reported in this context, there is a lack of systematic studies on the synthesis approaches, which involve cumbersome procedures such as seeds, templates [9–13,15], organic solvents [14], electrochemical reactions [19], photo-irradiation [20,21], toxic chemicals [22], or limitation of protecting reagents [23–25].

In this study, we developed a simple and versatile method to prepare anisotropic nanoparticles without using seeds or templates. We considered the method also from the viewpoint of green chemistry [26]. To accomplish these objectives, we studied the catalytic behavior of Au nanoparticles (AuNPs) to decompose peroxides [27,28]. Hydrogen peroxide was selected as a convenient reducing agent in an aqueous system. The effects of protecting agents on the synthesis of confeito-like AuNPs were examined. Moreover, the surface-enhancing effects of the obtained nanoparticles on Raman spectra were evaluated. The results obtained from these studies are useful for designing anisotropic nanoparticles with desirable plasmonic properties for sensors, optoelectronic devices, and other applications.

2. Materials and methods

2.1. Reagents

Sodium tetrachloroaurate(III) dihydrate ($NaAuCl_4{\cdot}2H_2O$, 99%) and Pluronic F-127 (a polyethylene oxide–polypropylene oxide–polyethylene oxide block copolymer, PF127) were purchased from Sigma Aldrich Co. (USA). Hexadecyltrimethylammonium bromide (HTAB) was obtained from Tokyo Chemical Industry Co. (Japan). Anhydrous citric acid (Cit), polyvinylpyrrolidone (PVP, average M.W.: 58,000), sodium hydroxide (NaOH), sodium dodecyl sulphate (SDS), rhodamine 6G (R6G), and an aqueous 35 wt% solution of hydrogen peroxide (H_2O_2) were purchased from Acros Organics (USA). All chemicals were of reagent grade and were used without further purification. Ultrapure (Millipore Milli-Q) water with a resistivity of 18 MΩ cm was used throughout all the syntheses and measurements in the study.

2.2. Synthesis of AuNPs

The synthesis of AuNPs was performed in a 50 cm^3 glass vial at ambient temperature. Specifically, 4 cm^3 of an aqueous 1 mM solution of $NaAuCl_4$ was diluted with 28 cm^3 of water, and a specified amount of the protecting agent (40.0 mg for PVP, PF127, SDS, and HTAB, or 16.0 mg for citric acid) was dissolved in the solution. An aqueous solution of H_2O_2 (80 mm^3) was added to the solution, and 8 cm^3 of an aqueous 100 mM solution of NaOH was then added with vigorous stirring. After 5 min, the stirring was slowed down and continued for 1 h. The reaction solution was allowed to stand overnight for the reaction to go to completion, and a dispersion of AuNPs was obtained.

2.3. Instruments

Transmission electron microscopy (TEM) images were acquired with a Hitachi H-7000 instrument at an accelerating voltage of 100 kV. The dispersion of AuNPs was poured on a carbon-coated copper grid, air-dried, and then used for the observation. The scanning electron microscopy (SEM) images were obtained with a JEOL JSM-6500F microscope. Ultraviolet–visible–near infrared (UV–vis–NIR) absorption spectra were recorded with a JASCO V-670 spectrophotometer with a quartz cell with a 1 cm light path. The SERS measurement was performed with a Raman Microprobe (Kaiser Raman Rxn1 Raman spectrometer with a TE-cooled CCD detector and holographic notch filters). The SERS excitation was provided by 785 nm radiation from an Invictus laser with a laser power of 100 mW.

2.4. Measurement of SERS

An anodized alumina filter (Anodisc 13, Whatman International Ltd., diameter: 13 mm, pore size: 0.02 μm) was assembled in a holder and fitted to a syringe (2 cm^3). The dispersion of AuNPs (2 cm^3) was loaded into the syringe and slowly filtered. The residual material on the filter was washed five times with 2 cm^3 of water without dismounting the filter, and then the filter was taken out to be air dried. To attach R6G to the AuNP-mounted filter, the filter was immersed in an aqueous solution of R6G (1 mM, 2 cm^3) for 2 h. Then, it was removed from the solution and placed on a silicon substrate with a cover glass on top. After focusing the Raman microscope on the residual material at 50-fold magnification, the Raman spectrum of the specimen thus prepared was recorded at an *exposure* time of 5 s and an accumulation of 10 scans.

3. Results and discussion

3.1. Characteristics of Au nanoparticles reduced by H_2O_2

The reduction reaction of $[AuCl_4]^-$ by H_2O_2 was facilitated in alkaline conditions [28] as shown in the chemical Eqs. (1) and (2).

$$H_2O_2 + 2OH^- \rightarrow O_2 + 2H_2O + 2e^- \quad (1)$$

$$[AuCl_4]^- + 3e^- \rightarrow Au^0 + 4Cl^- \quad (2)$$

Although the reaction solution did not change its appearance in the absence of NaOH, it turned bluish, with an induction period of several seconds to several minutes, after the addition of NaOH. The induction period varied depending on the protection agents used in the reaction; citric acid had the shortest period (several seconds), and SDS resulted in the longest period (several minutes). The difference in induction periods should depend on the adsorption behavior of the protecting agents during the nucleation and growth stages of AuNPs. The induction period and the subsequent rapid change of color suggest that the reaction progresses in stages and that the formation of nanoparticles is autocatalytic. Previous reports of the catalytic decomposition activity of AuNPs toward peroxides support this observation [27,28].

Although the color change of the solution was complete within 1 h, a small amount of bubbling continued for several hours because of the decomposition of excess H_2O_2. Then, the reaction mixtures were allowed to stand overnight to consume the remaining H_2O_2 and to obtain the AuNPs. The colored dispersion of AuNPs with protecting agents (X-AuNP; X represents the protecting agent) and that of an AuNP prepared by a conventional method (conv-AuNP) [29] are shown in Fig. 1.

The morphologies of AuNPs were observed by TEM and SEM (Fig. 2). While the conv-AuNP had polyhedral structures with diameters of 10–20 nm, all of the AuNPs obtained by the reaction with

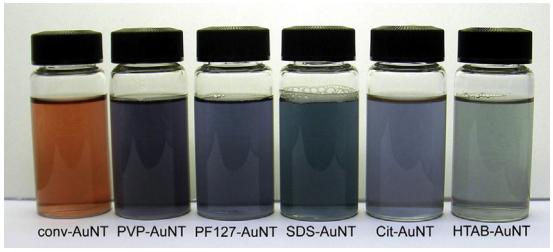

Fig. 1. Colored dispersions of AuNPs. All dispersions are at the same concentration (0.1 mM per Au atom). (For interpretation of the references to color in this figure legend, the reader is referred to the web version of the article.)

H_2O_2 were confeito-like particles with diameters in the range of tens to hundreds of nanometers (Fig. 2A). Additionally, in the case of HTAB–AuNP, bouquet-like structures were observed (Fig. 2B).

The mechanism of these structures were explained that the formation of $AuCl_{4-x}(OH)_x^-$ in the alkaline condition slowed the reduction reaction and led to the aggregation of nuclei in the nucleation stage [22,23]. Although the synthesis of AuNPs using H_2O_2 as a reducing agent was reported, the obtained AuNPs in neutral condition were just branched to three arms and the yield was not high [30]. In this study, the reaction solution was strongly alkaline (pH ~11), and then, there was enough time to allow aggregation of nuclei. The existence of induction periods supports this mechanism. The multi-core structures were formed in this induction period to be the confeito-like structures, and the strong alkaline condition facilitated the decomposition of H_2O_2 and successive particle growth. Furthermore, the autocatalytic reaction could play an important role to form the extended structures, because the catalytic activity of smaller AuNPs is higher than that of larger AuNPs [27]. The decomposition of H_2O_2 and the reduction reaction could be facilitated at the small nuclei, and the crystal growth would slow down as the vertices of AuNPs with high curvature become minor. Therefore, the radial dendrites would be formed with narrow size distribution.

Although the AuNPs obtained by this method have spherical shapes, the detailed structures of their surface differ depending on the protecting agents used. This observation suggests that the crystal growth was controlled by the adsorbates on the nanoparticles, as described previously [31,32]. The surfaces of AuNPs adsorb the coexisting chemical species by the ionic interactions and/or the hydrophobic interactions. The structures and ionic characteristics of adsorbates result in the specific interactions with the different facets of AuNPs as the adsorption face. This selective protection led

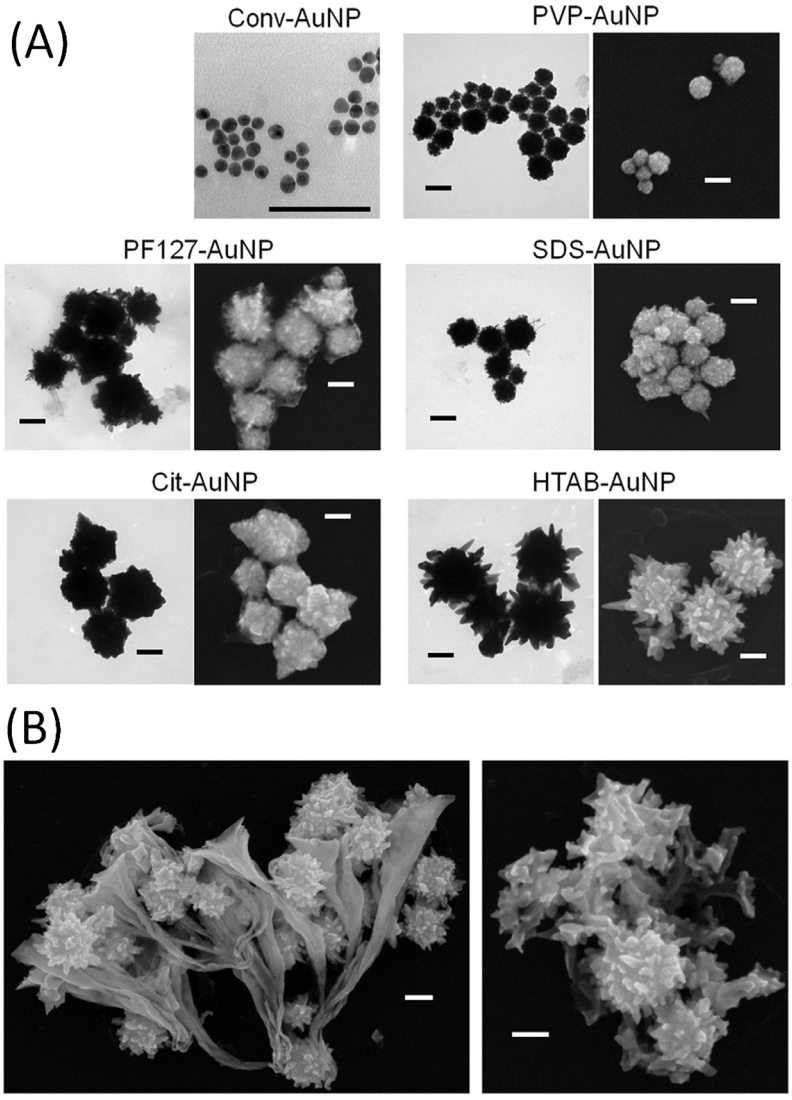

Fig. 2. (A) TEM (left) and SEM (right) images of AuNPs. (B) SEM images of HTAB–AuNPs. Each scale bar represents 100 nm.

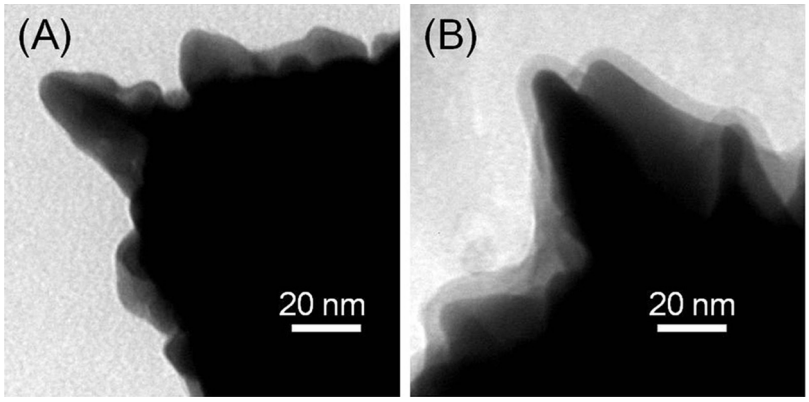

Fig. 3. TEM images of AuNPs. (A) Cit–AuNP and (B) HTAB–AuNP.

to the anisotropic crystal growth. For example, polymers adsorb easy but the protection effect of small molecules will be low.

In the TEM images, low-density layers of approximately 5–6 nm thickness were observed on the periphery of the HTAB–AuNPs, while the layer was slightly found on the Cit–AuNPs (Fig. 3, see also Fig. S1 in supplementary material). The layers on the HTAB–AuNPs were considered to be the adsorbed layers that consisted of one bilayer of HTAB molecules. This difference in layer formation clearly demonstrates that each protecting agent caps the surface of AuNP differently (see Figs. S1–S4 in supplementary material).

In the synthesis method developed in this study, various protecting agents can be chosen to design the shape of confeito-like AuNPs. Thus, this method is convenient and versatile for the quantitative synthesis of confeito-like AuNPs. It does not require seeds or a template, whereas a previous study using H_2O_2 needed seed particles to obtain dendritic AuNPs [30,33]. Thus, the method in the present work also has advantages from the perspective of green chemistry; no organic solvent is used and the excess H_2O_2 would decompose after the reaction.

3.2. Effect of AuNPs on SERS

Optical behaviors were investigated for the obtained AuNPs. The UV–vis–NIR spectra are shown in Fig. 4. The plasmon absorption bands were observed in the following order (the numbers in parentheses are the band positions in the spectrum):

$$\text{conv-AuNP}\ (520\ \text{nm}) < \text{PVP-AuNP}\ (575\ \text{nm}) < \text{PF127-AuNP}\ (595\ \text{nm}) < \text{SDS-AuNP}\ (632\ \text{nm}) < \text{Cit-AuNP}\ (666\ \text{nm}) < \text{HTAB-AuNP}\ (695\ \text{nm})$$

This order seems to be consistent with the color of the dispersion of AuNPs (Fig. 1).

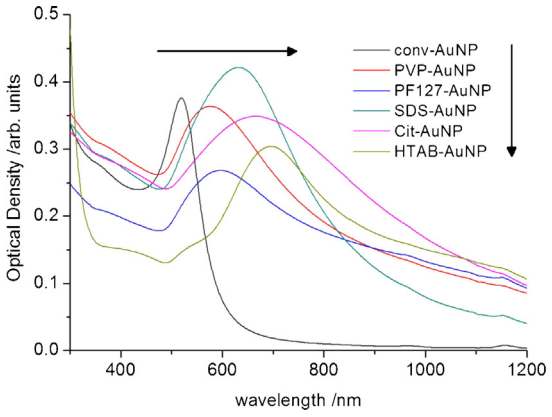

Fig. 4. UV–vis–NIR spectra of AuNPs. Each specimen is at the same concentration (0.1 mM per Au atom).

It is known that plasmon absorption bands shift as a function of the size (for spherical nanoparticles [34,35]) and of the aspect ratio (for nano-rods [36,37]), as well as by the interparticle interaction [38]. In the case of the AuNPs in the present study, the volume fraction (V_F) is estimated with the formula below:

$$V_F = \frac{\text{atomic weight of Au}\,(197.0) \times \text{concentration of Au}\,(1.0 \times 10^{-4}\,\text{M})}{\text{density of bulk Au}\,(19.3\,\text{g/cm}^3)} = 1.0 \times 10^{-6} \quad (3)$$

The V_F is small enough for the interparticle interaction to be negligible. The size and shape of an AuNP should mainly affect its plasmon absorption band and the color of the dispersion.

The SERS of R6G was measured on the AuNP specimen that was prepared as described in Section 2. The obtained spectra are shown in Fig. 5.

Because the Raman scattering from the R6G solution (20 mM) itself was very weak, a large amount of the solution was used for comparison in Fig. 5. Compared with the R6G solution, the AuNP specimen provided a strong Raman scattering, especially for the Raman bands at 1603 and 1648 cm^{-1} that are characteristics of R6G in the resonant SERS. These bands are corresponding to the stretching modes of aromatic rings in R6G, and a similarity between their vibration modes and the changes of molecular geometries between the ground states and the excited states leads to the effective enhancement [36,39].

It was found that the HTAB–AuNP and the Cit–AuNP resulted in strong enhancement of the R6G Raman bands (approximately 4 times that of the conv-ApNP), while the others showed weak

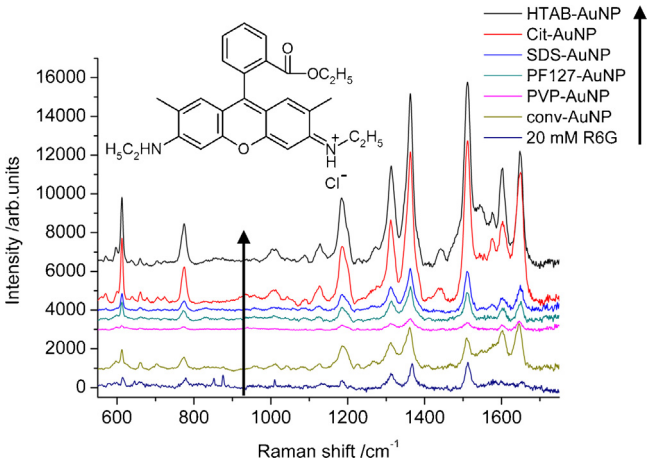

Fig. 5. The molecular structure of R6G and its SERS spectra obtained from the AuNP films.

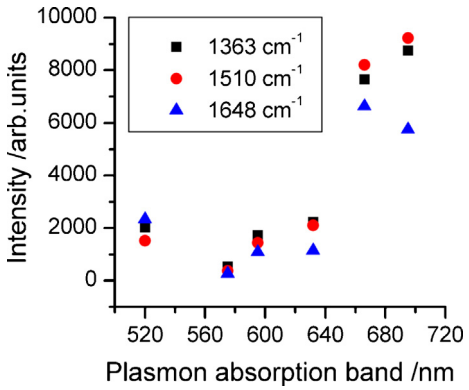

Fig. 6. Intensities of SERS at 1363, 1510, and 1648 cm^{-1} against the band positions of plasmon absorption of AuNPs.

enhancement. Incidentally, the order of the surface-enhancement factors in the series of confeito-like AuNPs is almost the same as that of the plasmon absorption band: the longer the resonance wavelength, the stronger the surface-enhancement effect. The intensities of several prominent bands in the SERS were plotted against the band positions of plasmon absorption (Fig. 6). This might be attributed to the resonance of the surface plasmon on the AuNP at the excitation wavelength (785 nm). The proximity of the wavelengths between the absorption band and the incident light allows strong coupling of the surface plasmon with the incident light to provide the strong electromagnetic field on the AuNP. Furthermore, the SERS indicated characteristics of the resonant SERS, e.g. the enhanced bands at 1440, 1603, and 1648 cm^{-1}. The R6G cannot resonate with the incident light at 785 nm, and the Raman scattering of a R6G solution without AuNPs was consistent with the non-resonant Raman scattering. Then, it was suggested that the energy state of R6G absorbed on the AuNPs shifted to enable to resonate with the incident light [39]. That is, the interaction between the R6G molecule with AuNP provided a new energy state, which was close to the excitation wavelength and led to the resonance of R6G. The band position of plasmon absorption of AuNPs could affect this new energy state of the R6G/AuNP complex, and then, the longer wavelength of plasmon absorption band provided the stronger SERS. According to the two-fold electromagnetic enhancement theory, the resonated R6G on AuNP could emit effectively the Raman scattering via the AuNP [40]. The excitation of R6G/AuNP complex was suggested by the broad band around 1500–1700 cm^{-1} in the spectra, especially for the Cit–AuNP and HTAB–AuNP: It was considered the enhanced fluorescence of the R6G/AuNP complex [40]. It is noted that the charge-transfer via the energy state of R6G/AuNP could also contribute the enhancing effect of the SERS [40,41].

Although the conv-AuNP had the shortest plasmon absorption band, its surface enhancement was superior to those of the PVP- and the PF127-AuNP and approximately the same as that of the SDS-AuNP. This observation could be explained by two factors. The conv-AuNPs changed to dark blue on the filter (which acted as a support for the particles), probably because of aggregation, and then their red-shifted plasmon absorption band became suitable for the SERS. Additionally, the larger total surface area of small conv-AuNPs compared with that of the other AuNPs allowed the adsorption of a higher number of R6G molecules on the surfaces. Because the diameter of conv-AuNP is approximately 1/5 that of PVP–AuNP, the total surface area of conv-AuNP could be 5 times larger than that of PVP–AuNP if compared as spheres. From this viewpoint, the weak enhancements of PVP- and PF127-AuNP might be due to their large sizes. Additionally, the diameter of conv-AuNP is 10–20 nm, which is suitable for producing a strong surface-enhanced effect [7]. This difference in diameters could explain the superiority of conv-AuNP for SERS.

The relative SERS band intensities of R6G with the confeito-like AuNPs were different from those with the conv-AuNP: the bands at 1184 cm^{-1} and 1648 cm^{-1} were rather weak. The weakness of the bands at 1184 and 1648 cm^{-1} might be explained by the orientation of the R6G molecules because these bands correspond to the transition moments of the xanthene ring in the direction of the long axis [41]. In terms of the surface selection rule [42], the long axis of the xanthene ring in the R6G molecule could be more parallel to the surface of confeito-like AuNPs than to the surface of conv-AuNPs. The R6G molecules attach to the surface of confeito-like AuNPs through the amine groups via an electrostatic interaction. These results indicate that the structures of the AuNPs might cause the difference in relative intensities between the confeito-like AuNP and the conv-AuNP. It was theoretically calculated that the localized surface plasmon would be concentrated on the tips on nanoparticles and act as the hot spots [37,43]. This effect increases significantly as the tips become sharp and intensify the electromagnetic field [43]. Moreover, it was reported that the localized surface plasmon raises the red-shift of the plasmon absorption bands [37]. Then, the confeito-like AuNPs, especially for the Cit–AuNPs and HTAB–AuNPs, could provide strong surface plasmon fields not only at the tips of the particles but also in the gaps between confeito-like particles, while the conv-AuNPs are contributed by only hotspots between adjacent particles [42]. The molecular orientation on the surface could be important in the case of confeito-like AuNPs because R6G molecules can be excited on the tips of confeito-like AuNPs without being disturbed by adjacent particles.

4. Conclusions

In an alkaline environment, $NaAuCl_4$ is reduced by H_2O_2, and this reduction results in confeito-like AuNPs with diameters of tens to hundreds of nanometers. The growth mechanism of these AuNPs could be attributed to an aggregation at the nucleation stage and an autocatalytic reduction of H_2O_2 by the AuNPs. Then the protecting agents can provide only the variation of detailed structures of the confeito-like AuNPs because of the selective adsorption of the agents onto the crystal faces of Au.

The AuNPs were also characterized in terms of optical properties. The confeito-like AuNPs were violet to blue and had broad and red-shifted plasmon absorption bands in the range of 570–700 nm, while the conv-AuNP had its plasmon absorption band around 520 nm. The confeito-like AuNPs that were prepared in aqueous solutions of HTAB and citric acid resulted in ~4 times stronger SERS compared with the conv-AuNPs. Although the other confeito-like AuNPs demonstrated SERS effects, their enhancing effects were smaller than those of the conv-AuNP. The order of enhancement factors corresponded to that of the plasmon absorption bands. These observations indicate that the plasmon absorption band is tunable using the structures of confeito-like AuNPs to obtain better surface-enhancing effects. Moreover, the confeito-like AuNPs resulted in different relative intensities of SERS bands compared with the conv-AuNP. This difference in intensities suggests that the adsorption orientation of R6G molecules on the confeito-like AuNPs is different from the orientation on the conv-AuNP.

In this study, a simple and versatile method for quick preparation of confeito-like AuNPs with different structures and optical properties was presented. This synthesis is a green method because the reducing agent used in this method will be decomposed finally to the water and oxygen, and the non-toxic protecting agents can be applied. The results obtained would be useful for designing plasmonic devices.

Supplementary data associated with this article can be found, in the online version, at http://dx.doi.org/10.1016/j.colsurfa.2013.07.003.

References

[1] S.A. Maier, H.A. Atwater, Plasmonics: localization and guiding of electromagnetic energy in metal/dielectric structures, J. Appl. Phys. 98 (2005) 11101.
[2] S. Eustis, M.A. El-Sayed, Why gold nanoparticles are more precious than pretty gold: noble metal surface plasmon resonance and its enhancement of the radiative and nonradiative properties of nanocrystals of different shapes, Chem. Soc. Rev. 35 (2006) 209–217.
[3] S.K. Ghosh, T. Pal, Interparticle coupling effect on the surface plasmon resonance of gold nanoparticles: from theory to applications, Chem. Rev. 107 (2007) 4797–4862.
[4] H. Metiu, Surface enhanced spectroscopy, Prog. Surf. Sci. 17 (1984) 153–320.
[5] Z.Q. Tian, B. Ren, D.Y. Wu, Surface-enhanced Raman scattering: from noble to transition metals and from rough surfaces to ordered nanostructures, J. Phys. Chem. B 106 (2002) 9463–9483.
[6] K. Ataka, Y. Hara, M. Osawa, A new approach to electrode kinetics and dynamics by potential modulated Fourier transform infrared spectroscopy, J. Electroanal. Chem. 473 (1999) 34–42.
[7] Z. Zhang, T. Imae, Study of surface-enhanced infrared spectroscopy. 1. Dependence of the enhancement on thickness of metal island films and structure of chemisorbed molecules, J. Colloid Interface Sci. 233 (2001) 99–106.
[8] J.A. Dieringer, K.L. Wustholz, D.J. Masiello, J.P. Camden, S.L. Kleinman, G.C. Schatz, R.P. Van Duyne, Surface-enhanced Raman excitation spectroscopy of a single rhodamine 6G molecule, J. Am. Chem. Soc. 131 (2009) 849–854.
[9] A. Manna, T. Imae, T. Yogo, K. Aoi, M. Okazaki, Synthesis of gold nanoparticles in a. Winsor II type microemulsion and their characterization, J. Colloid Interface Sci. 256 (2002) 297–303.
[10] M. Suzuki, Y. Niidome, Y. Kuwahara, N. Terasaki, K. Inoue, S. Yamada, Surface-enhanced nonresonance Raman scattering from size- and morphology-controlled gold nanoparticle films, J. Phys. Chem. B 108 (2004) 11660–11665.
[11] Y. Lu, G.L. Liu, J. Kim, Y.X. Mejia, L.P. Lee, Nanophotonic crescent moon structures with sharp edge for ultrasensitive biomolecular detection by local electromagnetic field enhancement effect, Nano Lett. 5 (2005) 119–124.
[12] V.S. Tiwari, T. Oleg, G.K. Darbha, W. Hardy, J.P. Singh, P.C. Ray, Non-resonance SERS effects of silver colloids with different shapes, Chem. Phys. Lett. 446 (2007) 77–82.
[13] L.H. Qian, X.Q. Yan, T. Fujita, A. Inoue, M.W. Chen, Surface enhanced Raman scattering of nanoporous gold: smaller pore sizes stronger enhancements, Appl. Phys. Lett. 90 (2007) 153120.
[14] J. Sharma, Y. Tai, T. Imae, Synthesis of confeito-like gold nanostructures by a solution phase galvanic reaction, J. Phys. Chem. C 112 (2008) 17033–17037.
[15] J. Sharma, T. Imae, Recent advances in fabrication of anisotropic metallic nanostructures, J. Nanosci. Nanotechnol. 9 (2009) 19–40.
[16] M. Suzuki, Y. Niidome, N. Terasaki, K. Inoue, Y. Kuwahara, S. Yamada, Surface-enhanced nonresonance Raman scattering of rhodamine 6G molecules adsorbed on gold nanorod films, Jpn. J. Appl. Phys. 43 (2004) 554–556.
[17] A.M. Schwartzberg, C.D. Grant, A. Wolcott, C.E. Talley, T.R. Huser, R. Bogomolni, J.Z. Zhang, Unique gold nanoparticle aggregates as a highly active surface-enhanced Raman scattering substrate, J. Phys. Chem. B 108 (2004) 19191–19197.
[18] C.J. Orendorff, A. Gole, T.K. Sau, C.J. Murphy, Surface-enhanced Raman spectroscopy of self-assembled monolayers: sandwich architecture and nanoparticle shape dependence, Anal. Chem. 77 (2005) 3261–3266.
[19] G. Duan, W. Cai, Y. Luo, Y. Li, Y. Lei, Electrochemically induced flowerlike gold nanoarchitectures and their strong surface-enhanced Raman scattering effect, Appl. Phys. Lett. 89 (2006) 211905.
[20] C. Hirano, T. Imae, Y. Yanagimoto, Y. Takaguchi, Photo-promoting fabrication of silver nanoparticles in the presence of anthracenyl-focal PAMAM dendrons, Polym. J. 38 (2006) 44–49.
[21] X. Luo, T. Imae, Shape-controlled synthesis of gold nanoparticles under UV irradiation in the presence of poly(ethylene glycol), Curr. Nanosci. 3 (2007) 195–198.
[22] G.H. Jeong, Y.W. Lee, M. Kim, S.W. Han, High-yield synthesis of multi-branched gold nanoparticles and their surface-enhanced Raman scattering properties, J. Colloid Interface Sci. 329 (2009) 97–102.
[23] Y. Ren, C. Xu, M. Wu, M. Niu, Y. Fang, Controlled synthesis of gold nanoflowers assisted by poly(vinyl pyrrolidone)–sodium dodecyl sulfate aggregations, Colloids Surf. A 380 (2011) 222–228.
[24] L. Wang, C.H. Liu, Y. Nemoto, N. Fukata, K.C.W. Wu, Y. Yamauchi, Rapid synthesis of biocompatible gold nanoflowers with tailored surface textures with the assistance of amino acid molecules, RSC Adv. 2 (2012) 4608–4611.
[25] L. Wang, M. Imura, Y. Yamauchi, Tailored synthesis of various Au nanoarchitectures with branched shapes, CrystEngComm 14 (2012) 7594–7599.
[26] J.A. Dahl, B.L.S. Maddux, J.E. Hutchison, Toward greener nanosynthesis, Chem. Rev. 107 (2007) 2228–2269.
[27] T. Kiyonaga, Q. Jin, H. Kobayashi, H. Tada, Size-dependence of catalytic activity of gold nanoparticles loaded on titanium (IV) dioxide for hydrogen peroxide decomposition, ChemPhysChem 10 (2009) 2935–2938.
[28] K.K. Dey, B.R. Panda, A. Paul, S. Basu, A. Chattopadhyay, Catalytic gold nanoparticle driven pH specific chemical locomotion, J. Colloid Interface Sci. 348 (2010) 335–341.
[29] J. Kimling, M. Maier, B. Okenve, V. Kotaidis, H. Ballot, A. Plech, Turkevich method for gold nanoparticle synthesis revisited, J. Phys. Chem. B 110 (2006) 15700–15707.
[30] E. Hao, R.C. Bailey, G.C. Schatz, J.T. Hupp, S. Li, Synthesis and optical properties of branched gold nanocrystals, Nano Lett. 4 (2004) 327–330.
[31] C.J. Murphy, T.K. Sau, A.M. Gole, C.J. Orendorff, J. Gao, L. Gou, S.E. Hunyadi, T. Li, Anisotropic metal nanoparticles: synthesis, assembly, and optical applications, J. Phys. Chem. B 109 (2005) 13857–13870.
[32] J. Gao, C.M. Bender, C.J. Murphy, Dependence of the gold nanorod aspect ratio on the nature of the directing surfactant in aqueous solution, Langmuir 19 (2003) 9065–9070.
[33] M. Zayats, R. Baron, I. Popov, I. Willner, Biocatalytic growth of au nanoparticles: from mechanistic aspects to biosensors design, Nano Lett. 5 (2005) 21–25.
[34] P.K. Jain, K.S. Lee, I.H. El-Sayed, M.A. El-Sayed, Calculated absorption scattering properties of gold nanoparticles of different size, shape, and composition: applications in biological imaging and biomedicine, J. Phys. Chem. B 110 (2006) 7238–7248.
[35] A. Manna, T. Imae, M. Iida, N. Hisamatsu, Formation of silver nanoparticles from a N-hexadecylethylenediamine silver nitrate complex, Langmuir 17 (2001) 6000–6004.
[36] A. Brioude, X.C. Jiang, M.P. Pileni, Optical properties of gold nanorods: DDA simulations supported by experiments, J. Phys. Chem. B 109 (2005) 13138–13142.
[37] F.H. Ho, Y.H. Wu, M. Ujihara, T. Imae, A solution-based nano-plasmonic sensing technique by using gold nanorods, Analyst 137 (2012) 2545–2548.
[38] M. Ujihara, J. Orbulescu, T. Imae, R.M. Leblanc, Film structures of poly(amido amine) dendrimers with an azacrown core and long alkyl chain spacers on water or Ag nanoparticle suspension, Langmuir 20 (2005) 6846–6854.
[39] P. Hildebrandt, M. Stockburger, Surface-enhanced resonance Raman spectroscopy of rhodamine 6G adsorbed on colloidal silver, J. Phys. Chem. 88 (1984) 5935–5944.
[40] K. Yoshida, T. Itoh, V. Biju, M. Ishikawa, Y. Ozaki, Experimental evaluation of the twofold electromagnetic enhancement theory of surface-enhanced resonance Raman scattering, Phys. Rev. B 79 (2009) 085419.
[41] H. Watanabe, N. Hayazawa, Y. Inouye, S. Kawata, DFT vibrational calculations of rhodamine 6G adsorbed on silver: analysis of tip-enhanced Raman spectroscopy, J. Phys. Chem. B 109 (2005) 5012–5020.
[42] M. Moskovits, Surface-enhanced Raman spectroscopy: a brief retrospective, J. Raman Spectrosc. 36 (2005) 485–496.
[43] H. Xu, J. Aizpurua, M. Käll, P. Apell, Electromagnetic contributions to single-molecule sensitivity in surface-enhanced Raman scattering, Phys. Rev. E 62 (2000) 4318–4324.